

Carbon Dots Induce Epithelial-Mesenchymal Transition for Promoting Cutaneous Wound Healing via Activation of TGF- β /p38/Snail Pathway

Zilin Wang, Lili Liu, Wenhuan Bu, Mengdan Zheng, Nianqiang Jin, Kai Zhang, Xiaowei Xu,* Ding Zhou,* Bai Yang, and Hongchen Sun*

Skin lesions, as a relatively common clinical manifestation, not only damage the skin's barrier function, but also affect the skin's ability to feel temperature, pain and touch. However, a highly efficient method to restore the morphology and function of damaged skin remains an unmet goal. In this work, carbon dots (CDots) with excellent biocompatibility are synthesized via microwave-assisted heating ascorbic acid and polyethyleneimine. The synthesized CDots can induce the epithelial-mesenchymal transition (EMT) process by activating transforming growth factor- β /p-38 mitogen-activated kinase/Snail signaling pathway, leading to an increase of cell motility. Further, by assessing a series of in vivo wound healing assays and histological examinations, it is demonstrated that CDots can accelerate the migration of epithelial cells in the full-thickness cutaneous wounds through EMT. As a result, a rapid re-epithelialization covers the granulation tissue and epidermal barrier formed, leading to a block of the external stimuli, reduction of the inflammatory reaction and the granulation tissue area, and finally the promotion of the wound healing with fewer scars.

been applied to promote cutaneous wound healing in present clinical studies, whereas these therapies still suffer from potential concerns related to high cost, difficult preservation of drugs or donors, immune rejection, and secondary damage to the donor sites.^[3–6,10] Cutaneous wound healing generally includes three phases: hemostasis and inflammation, tissue formation, and tissue remodeling, which overlaps each other to a certain degree without a precisely defined period of time.^[4,11,12] During the above phases, cell migration is a common phenomenon and plays a key role in cell recruitment and promoting wound healing.^[11–15] In the migration process, the epithelial cells transform to mesenchymal-like cells, which is known as an epithelial-mesenchymal transition (EMT) process and allows to rearrange the cytoskeleton, lose the cell–cell junctions and apical-basal polarity, enhance motility and invasiveness, and finally promote wound healing.^[12–17] Thus, it is significant to explore an effective way to induce EMT for increasing the migration of epithelial cells and further promoting cutaneous wound healing.^[15]

The materials currently used to induce EMT are mainly growth factors,^[4,17–20] which are expensive, complicated in extraction process, and difficult to store, resulting in a limited application and difficult to apply to a large scale.^[4–6]

1. Introduction

Cutaneous injury caused by trauma, burns, chronic wounds, and skin wound infection, is one of the most common clinical manifestations, which gives rise to pain, psychological stress and loss of quality life.^[1–4] Numerous strategies,^[5] including growth factor,^[6] gene therapy,^[7] cell therapy,^[8] and skin grafts,^[9] have


Dr. Z. Wang, Dr. L. Liu, Dr. M. Zheng, Prof. X. Xu, Prof. H. Sun
Hospital of Stomatology
Jilin University
Changchun 130021, P. R. China
E-mail: xiaoweixu@jlu.edu.cn; hcsun@jlu.edu.cn

Dr. Z. Wang, Dr. L. Liu, Dr. M. Zheng, Prof. X. Xu
Jilin Provincial Key Laboratory of Tooth Development
and Bone Remodeling
Jilin University
Changchun 130021, P. R. China

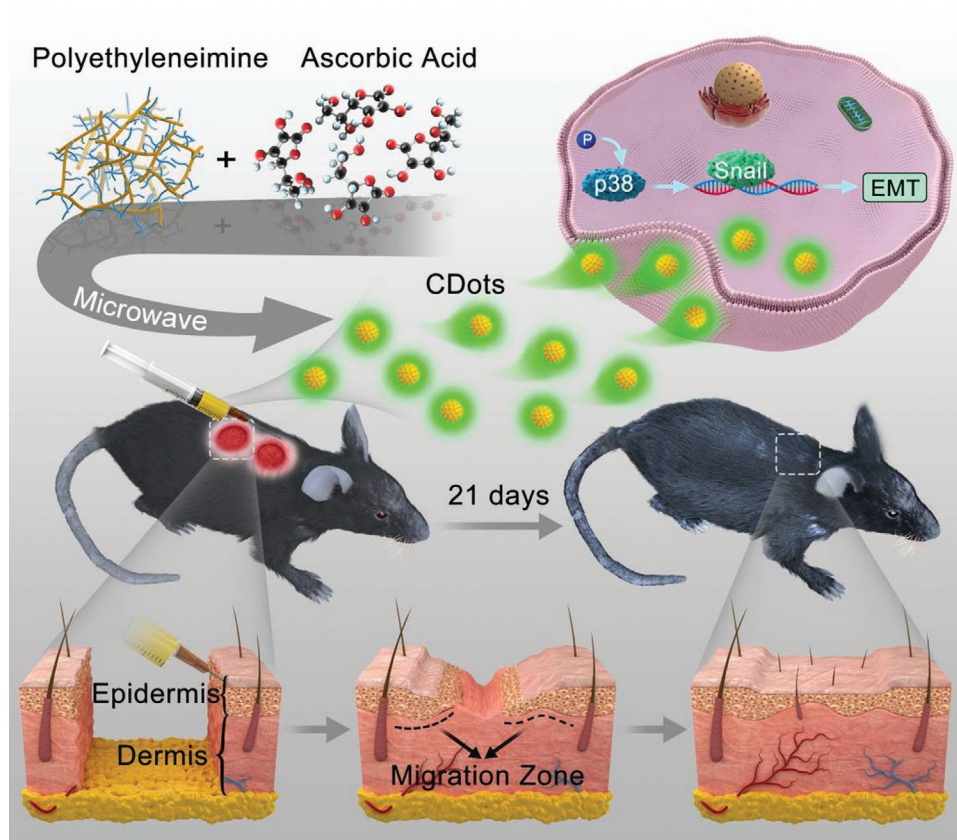
Dr. W. Bu, Dr. N. Jin
School and Hospital of Stomatology
China Medical University
Shenyang 110122, P. R. China

Prof. K. Zhang, Prof. B. Yang
State Key Laboratory of Supramolecular Structure and Materials
College of Chemistry
Jilin University
Changchun 130012, P. R. China

Prof. D. Zhou
State Key Laboratory of Luminescence and Applications
Changchun Institute of Optics
Fine Mechanics and Physics
Chinese Academy of Sciences
Changchun 130033, P. R. China
E-mail: zhouding@ciomp.ac.cn

 The ORCID identification number(s) for the author(s) of this article can be found under <https://doi.org/10.1002/adfm.202004886>.

DOI: 10.1002/adfm.202004886



Scheme 1. Schematic illustration of the preparation of CDots and their application in promoting wound healing through EMT via activation of TGF- β /p38/Snail pathway.

Nanomaterials as a nanoscale material, have several specific advantages, such as easy preparation, low cost, long-term preservation, and abundant surface groups, especially small size, which is beneficial to enter the living body.^[10,21] Nanoparticles have been clarified to play an important role in the process of EMT.^[5,22–28] For instance, titanium dioxide nanoparticles could induce the EMT process in colorectal cancer cells and hasten the progression of cancers.^[22] Multiwalled carbon nanotubes could directly induce EMT in human bronchial epithelial cells, which is related to the occurrence of pulmonary fibrosis.^[23–27] If the nanomaterial-induced EMT can be applied to tissue regeneration and wound healing, it will be of higher value.^[10] Carbon dots (CDots) are less than 10 nm carbon-based nanoparticles with several distinct merits, such as low cytotoxicity, abundant raw material, easy preparation, and fluorescence properties, thus showing great potential in various biomedical applications, including anti-inflammation,^[29] bacteriostasis,^[30] bioimaging^[31] and so on.^[32–47] Meaningfully, through neutralizing the reactive oxygen species from inflammation/infection and sterilizing the bacteria in the wounds, CDots could be utilized to accelerate wound healing.^[48,49] Despite these achievements, however, only the contaminated and dirty-infected wounds usually need antibacterial treatment,^[50] but a rapid re-epithelialization of the wound surface for forming the epidermal barrier is significant in various wounds. As a result, the exploitation of preparing CDots that are capable

of inducing EMT and therewith enhancing the cell motility is expected to make up for the shortcomings of traditional treatment methods.

In this work, CDots, which were synthesized from ascorbic acid and polyethyleneimine (PEI) by microwave-assisted heating strategy, have been developed and characterized for treating the full-thickness cutaneous wound. The as-prepared CDots with abundant carboxyl and amine groups exhibited excellent biocompatibility can induce the EMT process by activating transforming growth factor- β (TGF- β)/p-38 mitogen-activated kinase (p38)/Snail signaling pathway, resulting in the increased cell migration. In vivo studies revealed that CDots could accelerate the migration of epithelial cells in the full-thickness cutaneous wounds through triggering EMT, leading to a rapid re-epithelialization covering the granulation tissue and the formation of epidermal barrier thereof, all of which can block the external stimuli, reduce the inflammatory reaction and the granulation tissue area, and finally promote the wound healing with fewer scars (**Scheme 1**).

2. Results and Discussion

2.1. Synthesis and Characterization of CDots

In this study, CDots were prepared from ascorbic acid and PEI by a one-step microwave-assisted heating method. During

this process, the dehydration condensation of ascorbic acid and PEI and subsequent carbonization led to the formation of CDots (Scheme 1). To account for materials properties, the high-resolution transmission electron microscope (HRTEM) image (Figure 1a) was obtained. Figure 1a indicates that CDots possess a uniform shape without apparent aggregation. The average diameter of CDots is 3.5 nm, and the lattice spacing is 0.21 nm, which is consistent with the (100) crystallographic facet of graphitic carbon.^[51] This nanometer size of CDots is favorable to the entry of CDots into the cell and thereby the exertion of

the pharmacological function of CDots. An energy dispersive spectrum (EDS) demonstrates that CDots are composed of C, N, and O. Of these, all the O and a portion of C belong to ascorbic acid, whereas all the N and the other portion of C originate from PEI (Figure S1, Supporting Information). To further reveal the formation mechanism and the chemical structure of CDots, Fourier transform infrared (FTIR) and X-ray photoelectron spectroscopy (XPS) characterizations were carried out. The FTIR spectrum of ascorbic acid exhibits a C=O stretching vibration at 1755 cm⁻¹, a C–O stretching vibration at 1025 cm⁻¹,

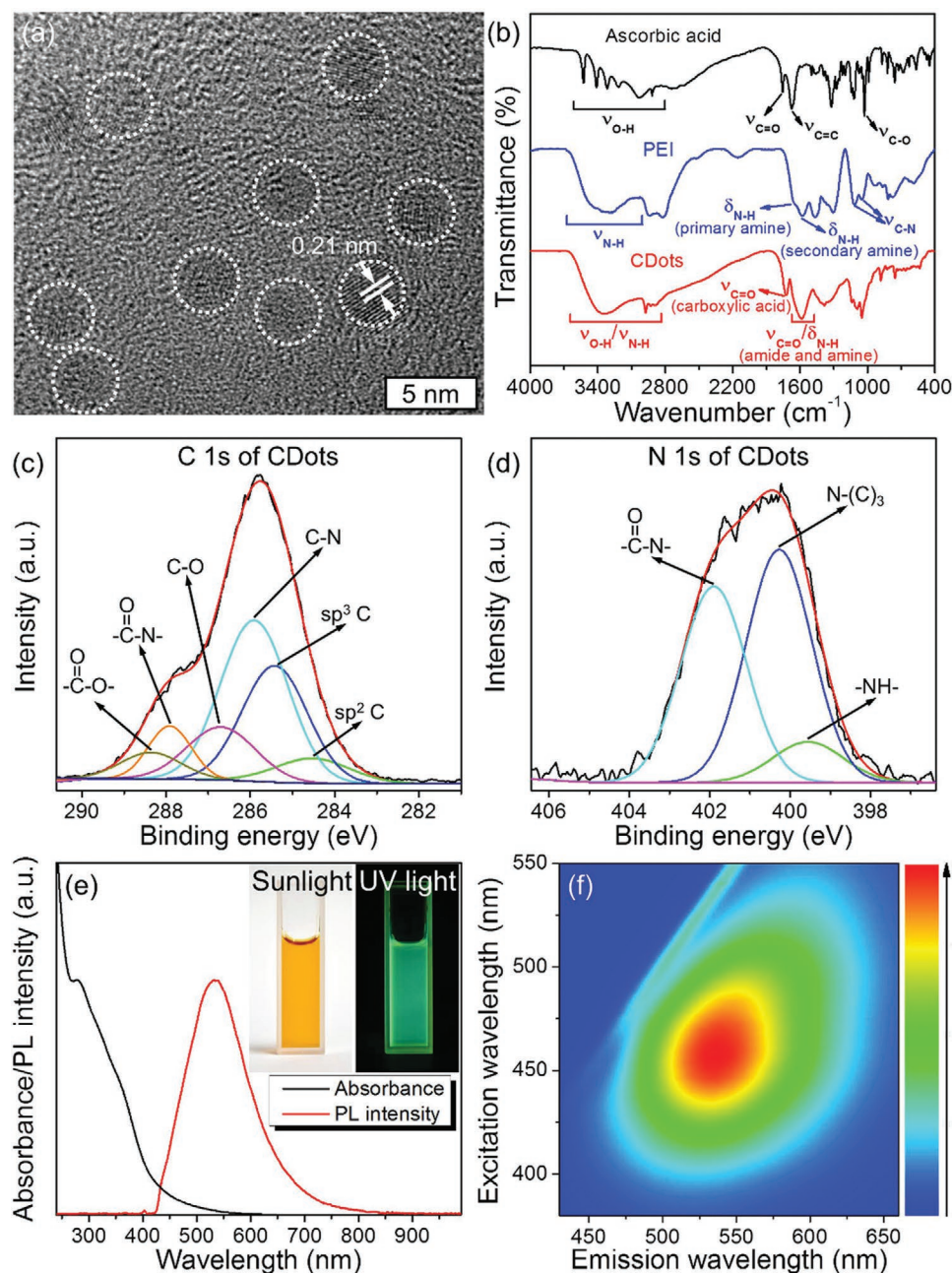


Figure 1. Characterizations of CDots. a) HRTEM image of CDots. b) FTIR spectra of ascorbic acid (black), PEI (blue), and CDots (red). c,d) High-resolution XPS spectra of CDots: c) C 1s and d) N 1s. e) UV-vis absorption (black) and PL emission spectra (red) of CDots. Insets: photographs of CDots solution taken under sunlight (left) and UV light (right), respectively. f) Excitation-emission map of CDots.

and a broad band of the O–H stretching vibration ranging from 2800 to 3600 cm^{-1} (Figure 1b), indicating the presence of carboxyl and hydroxyl groups. The FTIR spectrum of PEI presents two N–H bending vibrations at 1656 and 1581 cm^{-1} and also two C–N stretching vibrations located at 1123 and 1053 cm^{-1} . The two vibrations of each bond are attributed to the primary and secondary amines, respectively. The amine groups of PEI and the carboxyl/hydroxyl groups of ascorbic acid ensure the subsequent dehydration condensation and carbonization to form the CDots.^[51] The FTIR spectrum of the as-prepared CDots shows a C=O stretching vibration at 1720 cm^{-1} along with O–H/N–H stretching vibration at 2800–3600 cm^{-1} , suggesting the existence of the carboxyl and amine groups in CDots (Figure 1b). Besides, a relatively broad band appears at 1592 cm^{-1} , covering C=O stretching vibration (i.e., amide I band) and N–H bending vibration (i.e., amide II band). The broad band is mainly attributed to N–H bending vibration of free amine groups between the amide I and II band. These results demonstrate the formation of CDots is based on dehydration condensation and further carbonization between the carboxyl/hydroxyl and amine groups, and lots of carboxyl and amine groups are retained in CDots, which could be further proved by the following XPS characterizations.

As shown in Figure S2a (Supporting Information), the C 1s spectrum of ascorbic acid is fitted with four peaks centered at 284.5, 285.1, 286.3, and 288.3 eV that are attributed to sp^2 C, sp^3 C, C–O, and –COO–, respectively. The N 1s spectrum of PEI shows one peak centered at 399.7 eV (Figure S2b, Supporting Information), which is assigned to the N element in amine groups (–NH–). The C 1s spectrum of the as-prepared CDots shows six peaks at 284.5, 285.1, 285.8, 286.7, 287.8, and 288.3 eV (Figure 1c) that are attributed to sp^2 C, sp^3 C, C–N, C–O, –CON– and –COO–, respectively.^[46] The peak at 287.8 eV represents the amidation reaction between ascorbic acid and PEI, and the peak at 288.3 eV indicates the existence of carboxyl groups in CDots. Moreover, as compared to the N 1s spectrum of PEI, the N 1s spectrum of CDots shows three peaks at 399.7, 400.3, and 401.9 eV (Figure 1d and Figure S2b, Supporting Information), which are attributed to the –NH–, N–(C)₃, and –CON–, respectively, indicating amine-N (–NH–), dopant-N atoms (N–(C)₃) and amide-N (–CON–). In accordance with the results of FTIR analysis, the XPS characterizations also confirm the dehydration condensation and carbonization processes and the existence of carboxyl and amine groups in CDots.

Furthermore, the co-existence of carbonyl and amine groups is generally associated with amino acid groups. To determine whether the amino acid groups are present in CDots, the classical ninhydrin reaction has been carried out (Figure S3, Supporting Information).^[52] In ninhydrin reaction, amino acid groups can react with ninhydrin, resulting in the formation of the purple-colored product diketohydrindylidene diketohydrindamine, also known as Ruhemann's purple (RP), which has a maximum absorption at 570 nm. By evaluating the color change of the solution and measuring the absorption of RP, we can therefore prove whether the existence of the amino acid groups in CDots. As shown in Figure S3 (Supporting Information), we analyze the as-prepared CDots using the ninhydrin reaction and find that treatment with ninhydrin generates an obvious color change from light yellow to blue and a new absorption peak at 570 nm, suggesting the presence of amino acid groups in CDots.

The as-prepared CDots solution exhibits a strong photoluminescent (PL) emission, with the PL emission peak of our CDots centered at 533 nm under 405 nm excitation, and the apparent color of the solution is yellow under sunlight (Figure 1e). In contrast, the ascorbic acid and PEI aqueous solutions are colorless under sunlight and have no PL emission under ultraviolet (UV) light (Figure S4, Supporting Information), indicating the formation of CDots after the microwave treatment, which is also proved by the variations of their UV–vis absorption spectra (Figure 1e and Figure S4, Supporting Information). Furthermore, the excitation-emission map of the CDots aqueous solution presents that their main fluorescent color is green (Figure 1f), which is highly sensitive to naked eyes and beneficial to investigate the behaviors of CDots in biological systems therewith. All these results indicate that the as-prepared CDots possess several unique advantages, including nanometer size, abundant carboxyl and amine groups, and green fluorescence, for further use in biological applications.

2.2. Biocompatibility and In Vitro Cell Imaging of CDots

The evaluation for biocompatibility of CDots is needed for further in vivo and in vitro studies. Here, 3-(4,5-dimethyl-2-thiazolyl)-2,5-diphenyl-2-H-tetrazolium bromide (MTT) assay and apoptosis assay were used to investigate the biocompatibility of CDots. The result of MTT assay shows the viability of the human immortalized keratinocytes (HaCaT) cells treated with CDots is nearly unchanged even increasing CDots concentration to 600 $\mu\text{g mL}^{-1}$ (Figure 2a), indicating that CDots have nearly no effect on the proliferation of HaCaT cells (Figure 2a). Moreover, fluorescence-activated cell sorting (FACS) is carried out to investigate the effects of CDots on the apoptosis of HaCaT cells (Figure 2b). The result of apoptosis assay shows that there is no significant difference in the apoptosis of HaCaT cells treated by CDots with concentrations ranging from 0 to 600 $\mu\text{g mL}^{-1}$ (Figure 2b), demonstrating the excellent biocompatibility of CDots. Since PEI has remarkable cytotoxicity against HaCaT cells (Figure S5a, Supporting Information), the ultralow cytotoxicity of CDots suggests the complete removal of PEI after purification. By combining the results of MTT and apoptosis assays, the excellent biocompatibility of CDots is verified, and thus ensures its suitability for further in vitro and in vivo studies. To more directly observe the effects of CDots on cells, the green fluorescence of CDots is used for cell imaging (Figure 2c), which is seldom achieved by other conventional drugs. After incubating HaCaT cells with CDots of 600 $\mu\text{g mL}^{-1}$ for 24 h, the confocal laser scanning microscopy (CLSM) images were taken. It is interesting to note that a portion of CDots could be internalized into cells due to their nanosized diameter, whereas most of CDots are located around the cells (Figure 2c), implying the existence of some specific interactions between CDots and the HaCaT cell surface. In addition, the HaCaT cell morphology presents a variation from cuboidal cell shape to elongated cell shape, indicating a possible cell phenotype changes from epithelial phenotype to mesenchymal-like phenotype, which is consistent with the EMT process that caused several functional changes.^[5,11,18] However, because HaCaT cells could express a large number

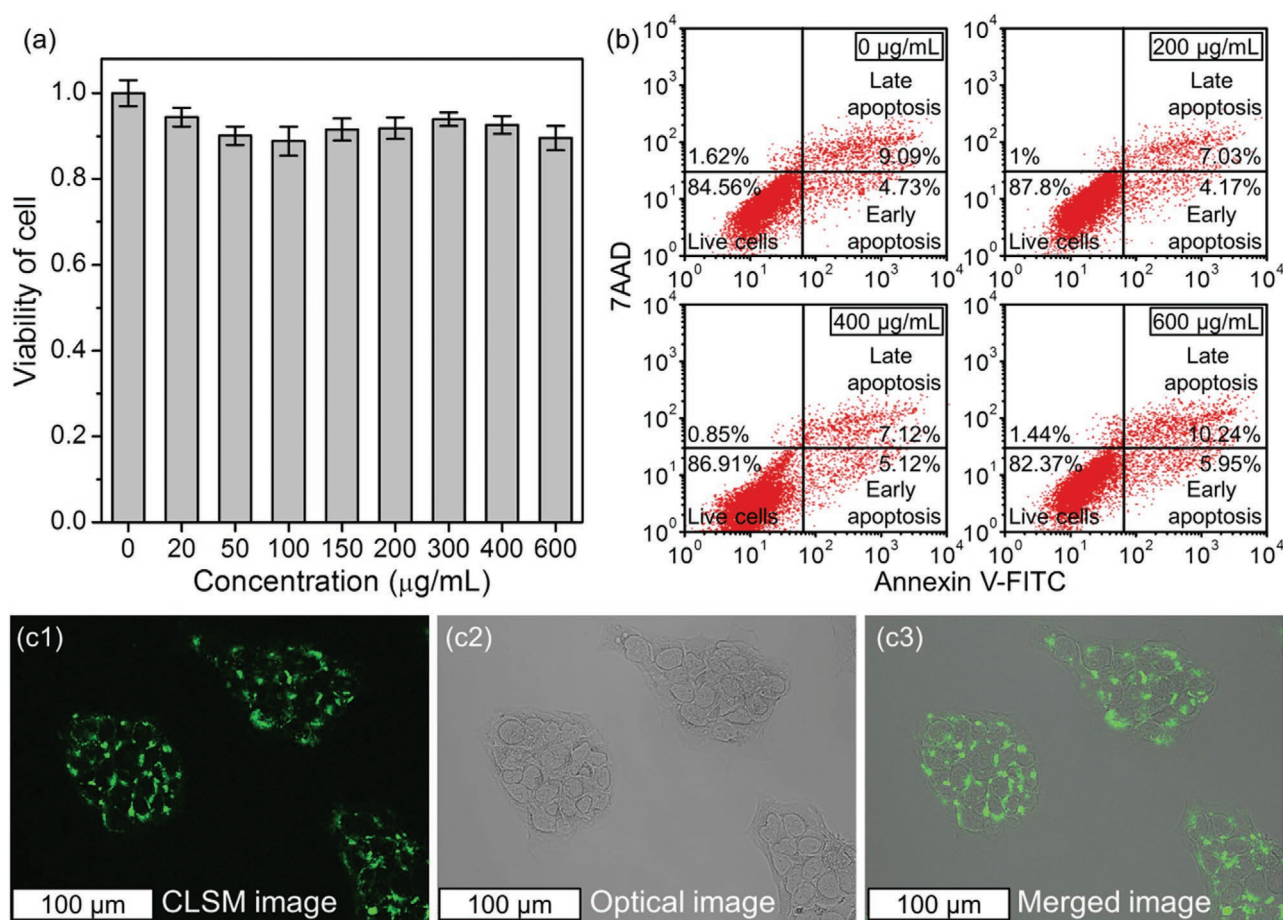


Figure 2. Cytotoxicity assays of CDots and cell imaging of CDots-treated HaCaT cells. a) MTT assay. HaCaT cells were treated with CDots at various concentrations of 20, 50, 100, 150, 200, 300, 400, and 600 $\mu\text{g mL}^{-1}$, respectively. b) FACS data of apoptosis assay. HaCaT cells were treated with CDots at various concentrations of 200, 400, and 600 $\mu\text{g mL}^{-1}$, respectively. c) Cell imaging of CDots-treated HaCaT cells. c1) CLSM image, c2) optical image, and c3) merged image of optical and CLSM images. Data are presented as mean \pm SD from three experiments.

of cell adhesion molecules (i.e., E-cadherin) during the proliferation, which could form the adherens junctions to bind cells with each other, HaCaT cells tend to aggregate and appear clumped in Figure 2c, which is well consistent with the result of the previous report.^[53] But just because of the confinement of the adhesion molecules, it makes the morphological variation of the HaCaT cells treated by CDots less obvious. Thus, HaCaT cells should be first digested by trypsin and then seeded into culture flasks for the detailed investigations of the morphological variation and the confirmation of EMT process.

2.3. CDots-Induced EMT

To clearly observe the morphological changes and confirm the EMT process, HaCaT cells are treated by CDots at different concentrations (i.e., 200, 400, and 600 $\mu\text{g mL}^{-1}$) for 24 h, then digested by trypsin, and dispersedly seeded into culture flasks again. As shown in Figure 3a, HaCaT cells without treatment by CDots maintain the epithelial cuboidal shape, while those treated by CDots exhibit the elongated fibroblastic morphology characteristic of mesenchymal cells. Furthermore, it can be

seen from the cell contours (black dash lines in Figure 3a) that the morphological variation tendency becomes more obvious as increase the concentration of CDots from 0, 200, 400, to 600 mg mL^{-1} , and the corresponding quantitative analysis also shows the aspect ratios of HaCaT cells increase from 1.5, 3.7, 5.3, to 9.0 as enhancing the concentration of CDots (Figure S6, Supporting Information), which is consistent with a transition from epithelial cuboidal shape to elongated fibroblastic shape, indicating the probable presence of CDots-induced EMT.^[17] It is worth mentioning that since the cytotoxicity of nanomaterials is reported to be able to cause similar morphological changes, CDots synthesized here are nearly nontoxic when its concentration is not higher than 600 $\mu\text{g mL}^{-1}$ (Figure 2a). Therefore, the morphological changes of HaCaT cells should not be induced by the cytotoxicity of nanomaterials, but by the pharmacological function of CDots themselves (i.e., CDots-induced EMT). To verify this hypothesis, molecular changes associated with EMT are evaluated through Western blot and immunofluorescence characterizations. After 24 h treatment with CDots, the expression of E-cadherin, as a well-known epithelial marker, presents a decreased level (Figure 3b,c), suggesting the loss of the adherent epithelial phenotype of HaCaT cells. In contrast, fibronectin and

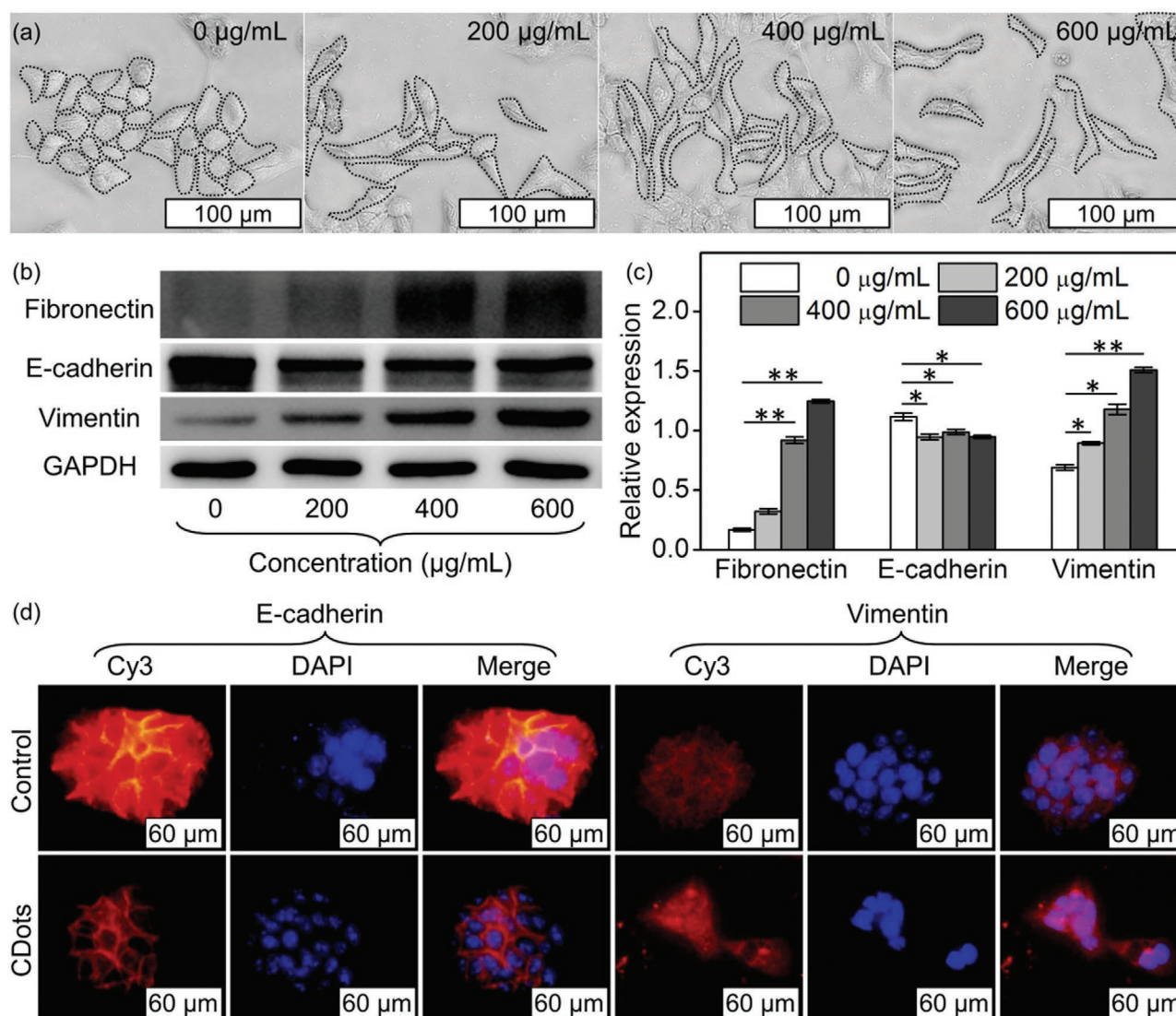


Figure 3. EMT of HaCaT cells induced by CDots. a) Morphological changes of HaCaT cells treated with CDots at various concentrations of 200, 400, and 600 $\mu\text{g mL}^{-1}$, respectively. b) Molecular changes associated with EMT: fibronectin, E-cadherin and vimentin analyzed by Western blot. c) Corresponding quantitative data from Western blot. The relative expressions are fibronectin/GAPDH, E-cadherin/GAPDH and vimentin/GAPDH, respectively. d) Immunofluorescence staining for E-cadherin and vimentin. Epithelial markers (E-cadherin staining, 1st and 3rd column, red fluorescence), mesenchymal markers (vimentin staining, 4th and 6th column, red fluorescence), and cell nuclei (DAPI staining, blue fluorescence) were observed by fluorescence microscopy. Data are presented as mean \pm SD from three experiments. * indicates $P < 0.05$; ** indicates $P < 0.01$.

vimentin as mesenchymal markers, their expression appears an obvious up-regulation, and HaCaT cells could express more fibronectin and vimentin when being treated by higher concentrations of CDots (Figure 3b,c), thus confirming CDots-induced EMT process in HaCaT cells. Consistent with the results of Western blot, the immunofluorescence also indicates a similar expression variation of E-cadherin and vimentin after being treated by 600 $\mu\text{g mL}^{-1}$ CDots. Compared to the control group, CDots treatment results in a significant decline of E-cadherin and an increase of vimentin, which further demonstrates CDots-induced EMT (Figure 3d).^[11] Based on these results, it is safe to conclude that CDots could promote the transition from epithelial phenotype to mesenchymal-like phenotype of HaCaT cells and thereof induce the EMT process.^[17]

One of the key features in EMT is the increase of cell motility,^[17] and thus HaCaT cells treated by CDots are expected to gain better cellular migration. Scratch assay and transwell assay are carried out to investigate changes in cell motility. In the scratch assay, HaCaT cells are seeded in a 6-well plate and cultured until complete confluence, and then a scratch is made with a pipette tip in each well, which is used to mimic the collective migration of HaCaT cells in wound healing in vivo to a great extent. As seen from Figure 4a,b, HaCaT cells without treatment by CDots exhibit only a little cell migration, whereas those co-cultured with CDots appear an evident dose-dependent cell migration, and 3.3-fold increase in cellular migration capability as the CDots concentration reaches 600 $\mu\text{g mL}^{-1}$. The increase in cell motility was also confirmed utilizing

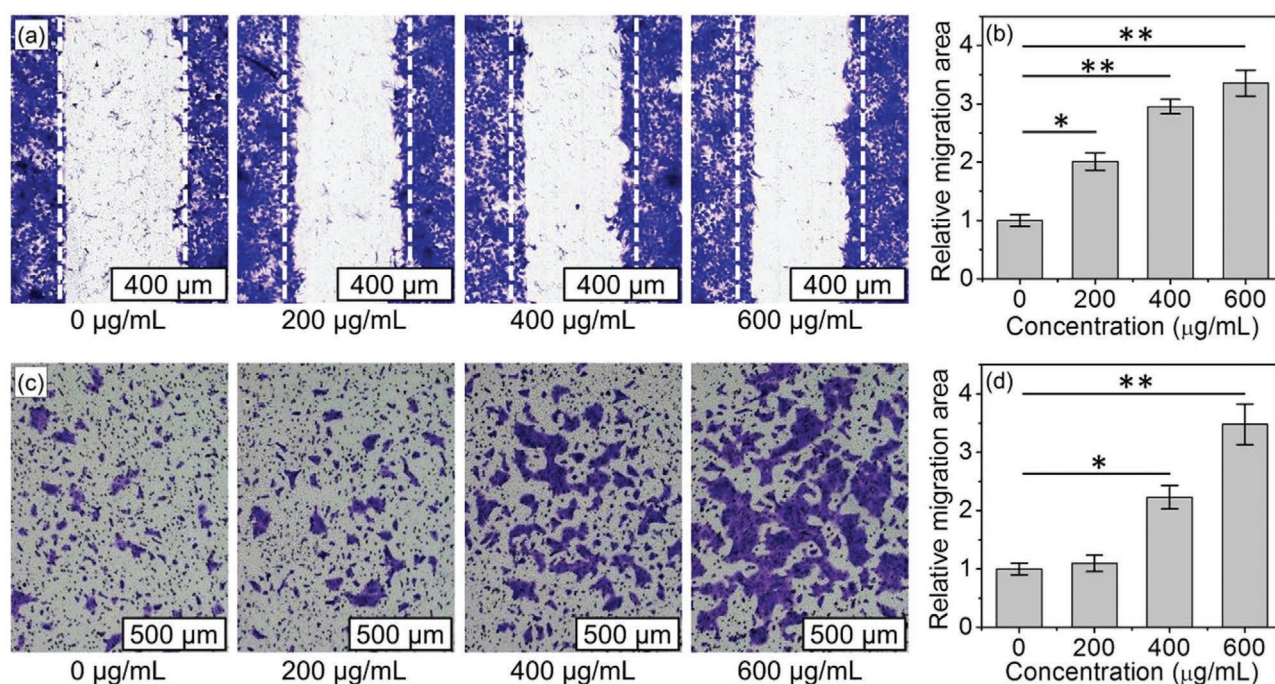


Figure 4. Cell motility of HaCaT cells treated with CDots. a) Scratch assay. Three parallel scratches were made with a pipette tip in each well and HaCaT cells were treated with CDots at various concentrations of 200, 400, and 600 $\mu\text{g mL}^{-1}$, respectively. Cells were stained with crystal violet and observed by microscopy. b) Corresponding quantitative data of scratched area was analyzed using ImageJ software. c) Transwell assay. Migration ability of HaCaT cells treated with CDots was also evaluated by transwell assay. The cells on inferior membrane were stained with crystal violet and observed by microscopy. d) Corresponding quantitative data of migrating area was analyzed using ImageJ software. Data are presented as mean \pm SD from three experiments. * indicates $P < 0.05$; ** indicates $P < 0.01$.

the transwell assay in which CDots (600 $\mu\text{g mL}^{-1}$) induced an ≈ 3.4 -fold increase of migrating cells as compared to the control (Figure 4c,d). Note that the increase of HaCaT cells in migration area and on the inferior membrane is not caused by cell proliferation, since CDots have no effects on the cell proliferation according to the cytotoxicity tests (Figure 2a). Besides, PEI and ascorbic acid are also applied to evaluate their effects on the cell motility. Figure S7a (Supporting Information) shows nearly no migrating cells on the inferior membrane in PEI group, which is reasonably attributed to the high cytotoxicity (Figure S5a, Supporting Information). Although ascorbic acid exhibits good biocompatibility (Figure S5b, Supporting Information), there are also few migrating cells on the inferior membrane in the ascorbic acid group (Figure S7b, Supporting Information). In all, CDots could induce the EMT process of HaCaT cells and therewith promote cell motility, showing a great potential in accelerating the wound healing, and the mechanism for inducing EMT should be closely related to the unique structure of CDots.^[15]

2.4. CDots-Induced Activation of TGF- β /p38/Snail Pathway

Having established that CDots can induce EMT, we next explored possible mechanisms underlying this process. Several studies have demonstrated that the EMT process induced by nanoparticles is generally realized by activating the TGF- β signaling pathway.^[22,23,25,26] To clarify the correlation between CDots-induced EMT and TGF- β pathway, the distribution of

CDots on the HaCaT cell surface should be first investigated, since the prerequisite for triggering TGF- β pathway is the activation of TGF- β receptors, and TGF- β receptors are located on the cell surface. In Figure 2c, it can be seen that CDots are mainly located around the HaCaT cells through CLSM images. To more clearly illustrate the correlation, fluorescence co-localization is applied to investigate the distribution of CDots and TGF- β receptors (Figure 5a). In experiments, TGF- β receptors are labeled by its primary antibody, and then the primary antibody is further combined with red fluorescent Cy3-labeled secondary antibody, so the TGF- β receptors can emit a red fluorescence under UV light excitation. Moreover, the nuclei of HaCaT cells are labeled with DAPI and show blue fluorescence. Therefore, Figure 5a shows that there are three kinds of fluorescent colors in the CLSM images: blue (nuclei) (Figure 5a2), red (TGF- β receptors) (Figure 5a3) and green (CDots) (Figure 5a4). More meaningfully, the green fluorescence of CDots is well overlapped with the red fluorescence of TGF- β receptors, indicating that they should be located in the same areas on the cell surface.

Generally, the increase of the expression level of the phosphorylated TGF- β receptors is the start of TGF- β pathway, so Western blot of detecting the level of the phosphorylated TGF- β receptors is carried out when treating HaCaT cells with CDots. As shown in Figure 5b,c, CDots could obviously increase the level of the phosphorylated TGF- β receptors. However, this result could also be caused by the CDots-promoted TGF- β expression, not the direct binding of CDots to TGF- β receptors. Therefore, the siRNA of TGF- β is applied

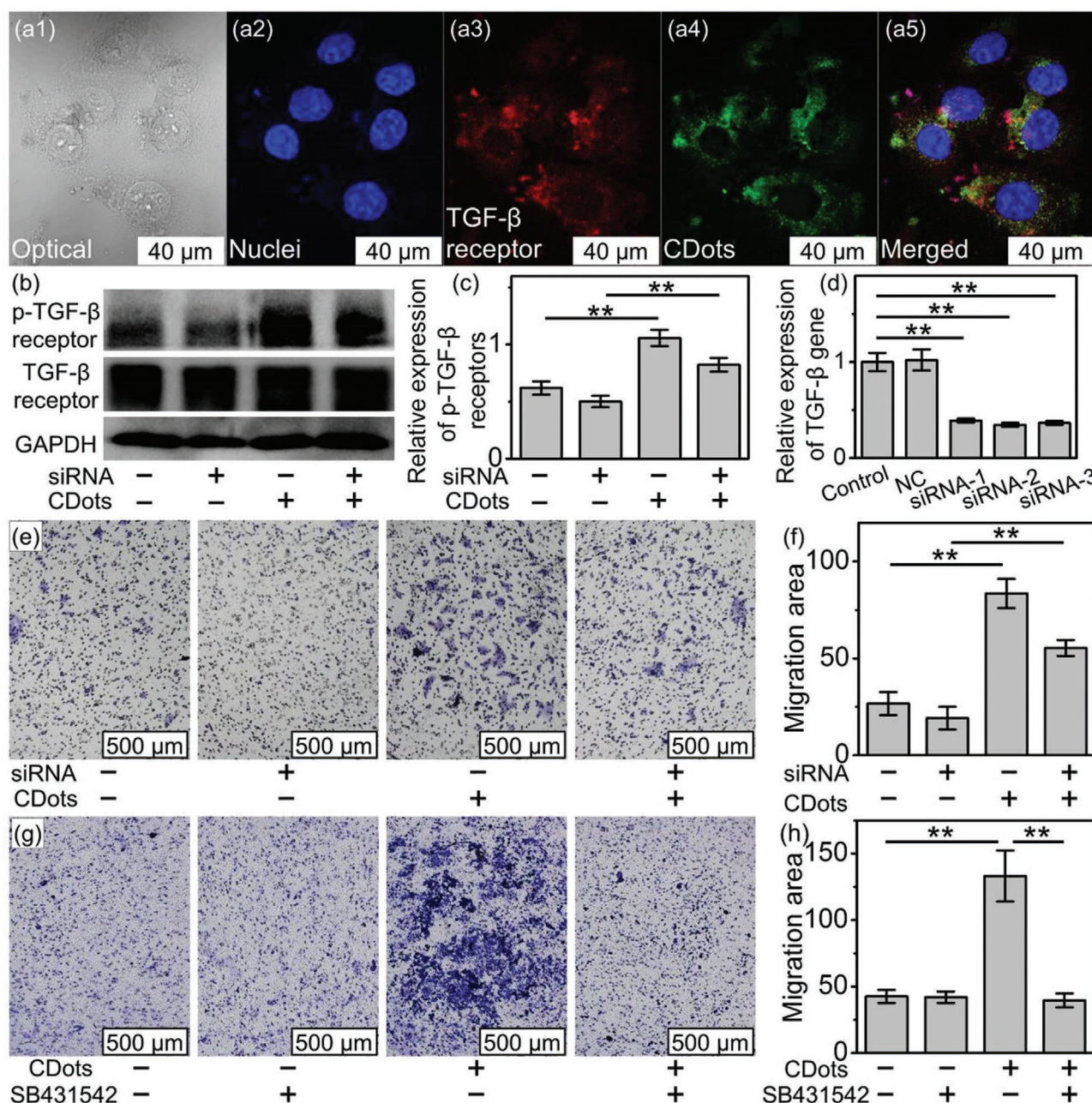


Figure 5. Phosphorylation of the TGF- β receptors induced by CDots. The fluorescence co-localization in HaCaT cells: CLSM images of a1) optical image, a2) cell nuclei (DAPI staining, blue fluorescence), a3) TGF- β receptors (red fluorescence), a4) CDots (600 $\mu\text{g mL}^{-1}$) (green fluorescence), and a5) merged image of CLSM images. b) Western blot assay of the phosphorylation of the TGF- β receptors. HaCaT cells were treated without or with CDots (600 $\mu\text{g mL}^{-1}$) and siRNA of TGF- β , respectively. c) Corresponding quantitative data from Western blot. The relative expression is p-TGF- β receptors/TGF- β receptors. d) qRT-PCR analysis of TGF- β mRNA level for detecting the transfection efficiency of siRNA-1, siRNA-2, and siRNA-3 of TGF- β in HaCaT cells. e) Transwell assay. Migration ability of HaCaT cells treated with siRNA of TGF- β and CDots (600 $\mu\text{g mL}^{-1}$) was evaluated by transwell assay. The cells on inferior membrane were stained with crystal violet and observed by microscopy. f) Corresponding quantitative data of migrating area was analyzed using ImageJ software. g) Transwell assay. Migration ability of HaCaT cells treated with TGF- β inhibitor SB431542 and CDots (600 $\mu\text{g mL}^{-1}$) was evaluated by transwell assay. The cells on inferior membrane were stained with crystal violet and observed by microscopy. h) Corresponding quantitative data of migrating area was analyzed using ImageJ software. Data are presented as mean \pm SD from three experiments. * indicates $P < 0.05$; ** indicates $P < 0.01$.

to knock down the expression of TGF- β in HaCaT cells and the effects of CDots on the level of the phosphorylated TGF- β receptors are further evaluated (Figure 5b–d). The results of Western blot indicate that after the knockdown of TGF- β ,

CDots can still increase the level of the phosphorylated TGF- β receptors. Meanwhile, transwell assay also indicates that CDots can still increase cell motility of HaCaT cells, demonstrating that CDots can still induce EMT even if TGF- β are

knocked down (Figure 5e,f). These results prove that CDots could interact with TGF- β receptors, and cause the phosphorylation of the TGF- β receptors thereof, leading to the activation of the TGF- β pathway. To further investigate the correlation between CDots-induced EMT and TGF- β pathway, SB-431542, the inhibitor of TGF- β receptors, is adopted to evaluate whether CDots-induced EMT could still be triggered by the TGF- β pathway. As seen from the results of the transwell assay (Figure 5g,h), sole SB-431542 would not change the cell motility of HaCaT cells, and HaCaT cells treated by CDots appear high cell motility due to CDots-induced EMT. However, after adding SB-431542, the cell motility of HaCaT cells treated by CDots drops down to the level of the control group (Figure 5g,h), demonstrating the suppression of CDots-induced EMT by SB-431542. Considering SB-431542 is an inhibitor of the TGF- β pathway, TGF- β pathway should play a pivotal role in CDots-induced EMT.^[19,54]

Moreover, TGF- β pathway contains two forms: canonical and non-canonical pathways, both of which could trigger EMT.^[55,56] Both of these two pathways were investigated to confirm the detailed mechanism of CDots-induced EMT. Here, HaCaT cells were first treated by CDots ($600 \mu\text{g mL}^{-1}$) for different time, and then the cell lysates at different time points (0, 0.25, 1, 2, 4, 8, 12, and 24 h) were examined by Western blot analysis. According to Figure 6a and Figure S8 (Supporting Information), phosphorylation levels of Smad2 and Smad3 were calculated and showed no significant difference at different time points, implying the canonical pathway was not

activated. On the other hand, phosphorylation levels of p38, extracellular regulated protein kinases (ERK) and c-Jun N-terminal kinase (JNK), which are the three main kinds of downstream signaling pathway factors in the non-canonical TGF- β pathway, are examined.^[56] The result shows there were nearly no variations in ERK and JNK (Figure S8, Supporting Information), while the phosphorylation level of p38 was found to be obviously up-regulated (Figure 6a,b), indicating the activation of p38 signaling pathway by CDots. But, after adding SB-431542, the phosphorylation level of p38 in HaCaT cells treated by CDots declines to the level of the control group (Figure 6d,e), suggesting that the CDots-activated p38 pathway should be originated from the TGF- β pathway, not from other upstream pathways. To further confirm the role of p38 pathway in CDots-induced EMT,^[19] 1-5-tert-butyl-2-p-tolyl-2H-pyrazol-3-yl)-3-[4-(2-morpholin-4-yl-ethoxy)naphthalen-1-yl]urea (BIRB 796), a highly potent p38 inhibitor which could inhibit phosphorylation of p38, was applied.^[57] As evidenced in Figure 7a,b, the phosphorylation level of p38 in HaCaT cells treated by CDots could be raised, while the phosphorylation level declines to the level of the control group after adding BIRB 796. Meanwhile, by adding BIRB 796, the expression level of fibronectin, E-cadherin and vimentin of HaCaT cells with treatment by CDots recovered to the normal level of the control group (Figure 7a,b) along with the decreased cell motility compared to those treated by CDots alone (Figure 7c,d), indicating that CDots-induced EMT is mainly conducted through the activation of p38 pathway.^[19]

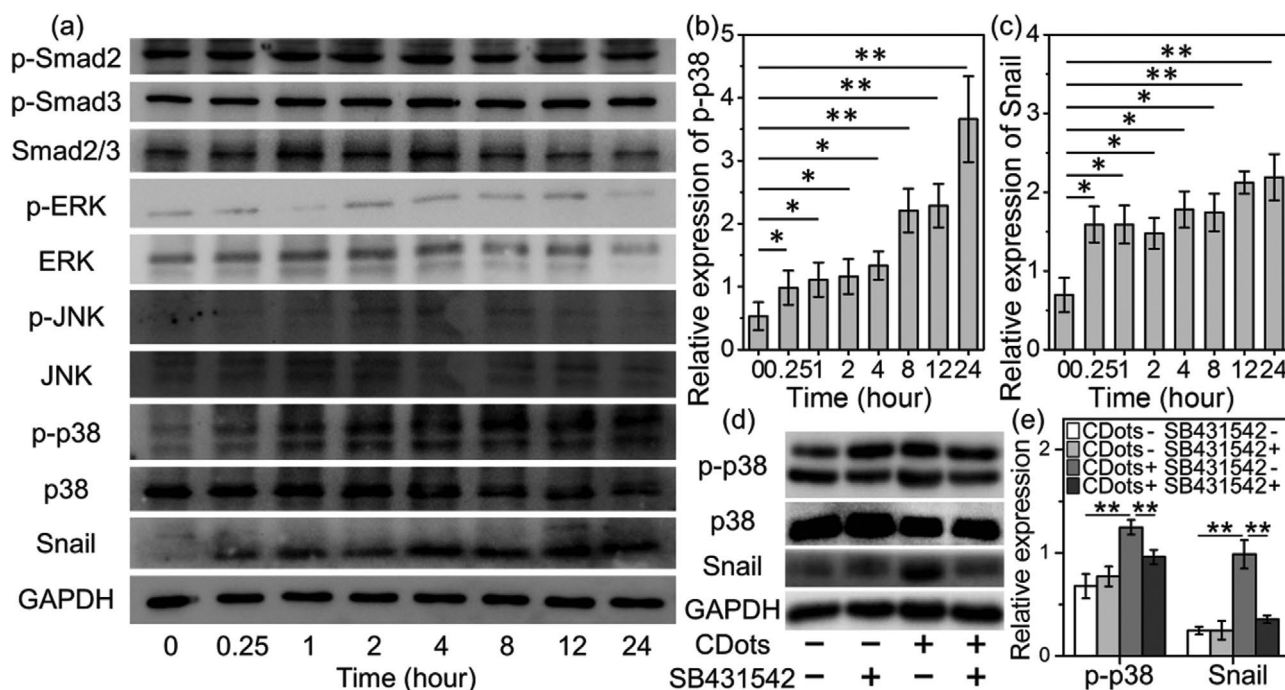


Figure 6. TGF- β /p38/Snail signaling pathway activated by CDots. a) Western blot assay of Smad signaling pathway-related proteins (Smad2 and Smad3), non-Smad signaling pathway-related proteins (ERK, JNK and p38), and Snail. Corresponding quantitative data of b) the phosphorylation level of p38 (i.e., p-p38/p38) and c) the expression of Snail (i.e., Snail/GAPDH) from Western blot. d) Western blot assay of p-p38, p38 and Snail. HaCaT cells were treated without or with CDots ($600 \mu\text{g mL}^{-1}$) and SB431542, respectively. e) Corresponding quantitative data of the phosphorylation level of p38 and the expression of Snail from Western blot. Abbreviations: p-Smad2, phosphorylated Smad2; p-Smad3, phosphorylated Smad3; p-ERK, phosphorylated ERK; p-JNK, phosphorylated JNK; p-p38, phosphorylated p38. “–” and “+” symbols represent “without” and “with,” respectively. Data are presented as mean \pm SD from three experiments. * indicates $P < 0.05$; ** indicates $P < 0.01$.

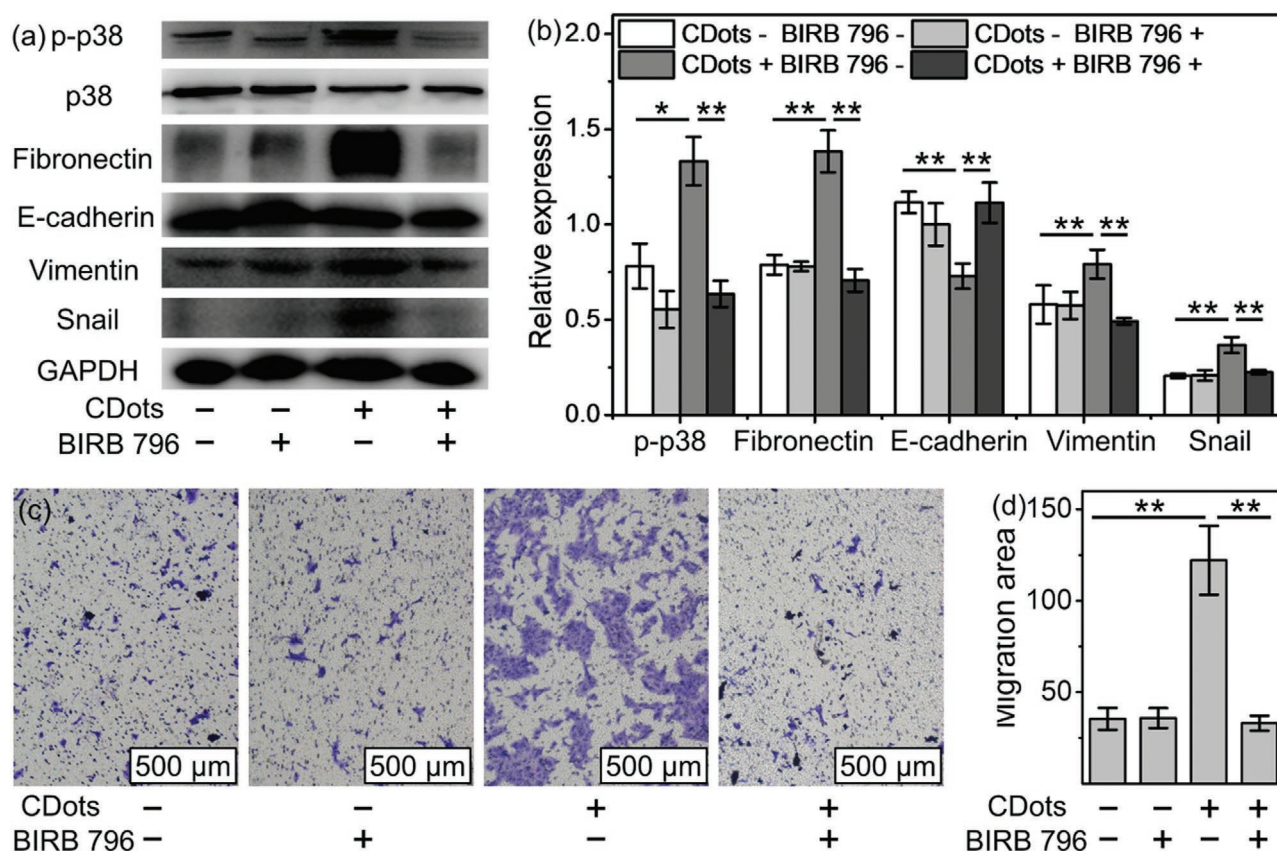


Figure 7. Snail and p38 involved in CDots-induced EMT. a) Western blot assay of p-p38, EMT-related proteins (fibronectin, E-cadherin, and vimentin) and Snail. HaCaT cells were treated without or with CDots ($600 \mu\text{g mL}^{-1}$) and BIRB 796, respectively. b) Corresponding quantitative data from Western blot. The relative expressions are p-p38/p38, fibronectin/GAPDH, E-cadherin/GAPDH, vimentin/GAPDH and Snail/GAPDH, respectively. c) Transwell assay. Migration ability of HaCaT cells treated with CDots ($600 \mu\text{g mL}^{-1}$) and BIRB 796 was evaluated by transwell assay. The cells on inferior membrane were stained with crystal violet and observed by microscopy. d) Corresponding quantitative data of migrating area was analyzed using ImageJ software. “–” and “+” symbols represent “without” and “with,” respectively. Data are presented as mean \pm SD from three experiments. * indicates $P < 0.05$; ** indicates $P < 0.01$.

The downstream effectors of p38 signaling pathway (i.e., the transcription factors), which could regulate gene expression to trigger EMT,^[19] are further revealed. On the basis of the Western blot and the corresponding quantitative analysis, Snail expression of HaCaT cells increases when extending the treatment time of HaCaT cells by CDots, proving that CDots-induced EMT is mainly caused by Snail (Figure 6a,c). Furthermore, it is found that when the phosphorylation of p38 is inhibited by BIRB 796, the Snail expression drops down to the level of the control group, demonstrating Snail is regulated by p38 signaling pathway (Figure 7a,b).^[57] Taken together, our findings suggest that CDots-induced EMT of HaCaT cells is triggered by activating TGF- β /p38/Snail pathway.

TGF- β is a multifunctional cytokine belonging to the TGF- β superfamily, which could bind to TGF- β receptors located at the cell surface.^[58,59] In TGF- β superfamily, cystine knot, which is composed of carboxyl and amine groups, is a hallmark of this ligand family, and could recognize TGF- β receptors.^[60,61] It is well established that the activation of the TGF- β pathway is reflected by the increase of the phosphorylation level of the TGF- β receptors, and the increase of the level of the phosphorylated TGF- β receptors is mainly due to the specific binding

of some substance containing cystine knot with TGF- β receptors.^[60,62] Therefore, the increased level of the phosphorylated TGF- β receptors of HaCaT cells treated by CDots could verify the presence of a cystine knot structure in CDots. According to FTIR and XPS analysis, there are lots of carboxyl and amine groups in our synthesized CDots (Figure 1b–d). The classical ninhydrin reaction further demonstrates the presence of amino acid groups in CDots (Figure S3, Supporting Information). Additionally, the fluorescence co-localization (Figures 2c and 5a) and the high level of the phosphorylated TGF- β receptors activated by CDots (Figure 5b) suggest the interactions between CDots and TGF- β receptors. All these results strongly indicate that the cystine knot structure is present in our CDots, leading to the recognition of TGF- β receptors by CDots, the further interaction with TGF- β receptors and the final activation of the TGF- β signaling pathway.^[60,63] This is why CDots could induce EMT, but ascorbic acid can't, because ascorbic acid possesses no amine groups. Besides, the size effect of CDots on triggering the TGF- β /p38/Snail pathway is examined. Another two kinds of CDots (named CDotsS1 and CDotsS2) with a size of 2–5.5 nm are prepared via a microwave-assisted strategy according to our previous reports.^[29,64] These two CDots are also

used to treat HaCaT cells in accordance with the procedures of treating HaCaT cells by CDots synthesized from ascorbic acid/PEI. The results of Western blot indicate that the level of the phosphorylation of TGF- β receptors, the phosphorylation of p38 and the expression of Snail are nearly unchanged (Figure S9a,b, Supporting Information), suggesting that although CDotsS1 and CDotsS2 possess similar size, they can't activate the TGF- β /p38/Snail pathway. To further prove this, the transwell assay is also adopted to evaluate the cell motility change of HaCaT cells treated by CDotsS1 and CDotsS2 (Figure S9c,d, Supporting Information), and the results show nearly no migrating cells on the inferior membrane in these two CDots groups, indicating that CDotsS1 and CDotsS2 are unable to induce EMT. These results demonstrate that the CDots-activated TGF- β pathway is because of a specific chemistry, not the size effect. Nevertheless, more detailed mechanisms of how CDots activate the TGF- β pathway and therewith induce EMT of HaCaT cells remain unclear, and more future studies are still needed to clarify and address this issue.

2.5. In Vivo Wound Healing Promoted by CDots and Histological Evaluation

Since the motility of HaCaT cell could be greatly enhanced by CDots, the application of CDots to wound in vivo is expected to accelerate the migration of epithelial cells for wound healing, which is important for re-epithelialization and reducing scar formation.^[11,65] Thus, to evaluate the ability of CDots to promote wound healing in vivo, male C57BL/6 mice (four to six-week-old) with full-thickness cutaneous wounds were randomly divided into two groups, namely control and CDots groups.^[66] As shown in Figure 8a, the representative digital photographs of the wounds in these two groups are taken on day 1, 7, 12, 15, 18, and 21, respectively. The images illustrate no significant difference among these two groups on day 1, while the CDots group achieves a significantly larger reduction in wound area as compared with the control group on day 7. Such a comparison of reduction in wound area becomes more apparent on day 12, namely, the wound healing rates are significantly accelerated by CDots. Figure 8b shows the quantification of the corresponding wound area upon different treatments. On day 12, compared to the initial wound area, the residual wound area of the CDots group has decreased to 17%, while the control group remains 31%. Meaningfully, on day 15, the wounds in the CDots group have almost healed up and few scars have formed (Figure 8b), whereas there is still large wound area in the control group (20%) (Figure 8b). Until day 21, the wound healing in the control group is completed, but accompanied by the massive scar formation (Figure 8a).^[67] These results demonstrate that CDots significantly accelerate the wound healing process owing to CDots-induced EMT.

To gain more insight into wound healing, the healing quality of the treated full-thickness cutaneous wounds, namely skin and the subcutaneous tissues around the wound areas, is assessed by hematoxylin and eosin (H&E) staining of the wound site tissue. As shown in Figure S10 (Supporting Information), H&E staining image of fresh wound shows the complete removal of the epidermal and dermal layers. On day 7,

the H&E staining image of the control group shows that no re-epithelialization is formed (red arrows in Figure 8c1), but there are considerable inflammatory cells and excessive granulation tissue existing in wound (red arrows in Figure 8c1), where plenty of scabs are connected to the granulation tissue (yellow arrows in Figure 8c1). In contrast, an obvious re-epithelialization and a balanced amount of granulation tissue can be observed in the CDots group (red arrows in Figure 8c4), the inflammatory cell infiltration underneath the epidermis is much smaller (Figure 8c4), and the scab has fallen off (yellow arrows in Figure 8c4). These data clearly demonstrate that CDots can accelerate the migration of epithelial cells through triggering EMT, and the epithelial cells (i.e., re-epithelialization) rapidly cover the granulation tissue,^[65] resulting in the formation of epidermal barrier, which can block the external stimuli and therewith reduce the inflammatory reaction and the overgrowth of the granulation tissue.^[11]

On day 15, due to the lack of epidermal barrier in the control group, excessive granulation tissues secrete excessive collagen under the external stimuli. These excessive collagen could form lots of broad, haphazardly arranged and brightly hypereosinophilic collagen fibers, and these collagen fibers are at varying angles with the wound surface (blue arrows in Figure 8c2), which are consistent with the previous literature.^[68] Meanwhile, in these disorganized collagen fibers, the occurrence of hyalinization could be observed (green arrows in Figure 8c2), which would result in the scar formation.^[67] However, in the CDots group, a reasonable amount of collagen is secreted (blue arrows in Figure 8c5), and nearly no hyalinization occurs, which is beneficial for the wound healing. More importantly, the wounds in the CDots group have almost healed up. To better clarify the differences in the quantities of the collagen, Masson's trichrome staining is performed (Figure S11, Supporting Information). Masson's trichrome staining is applied by immersion of the fixated sample into Weigert's iron hematoxylin and then with three different solutions, where the collagen stained with Masson's trichrome staining is cyan.^[69] Thus, by staining the tissues of the control and CDots groups with Masson's trichrome staining, the comparisons of the collagen expressions between the control and CDots groups on day 15 can be carried out, where the section thickness of each sample is identical for keeping the experiment parallel. Figure S11 (Supporting Information) shows that the area and contrast of the cyan regions in the control group is larger and darker than those of the CDots group, indicating that the collagen quantities of the control group are more than that of the CDots group, which is in accordance with the H&E staining. These results further indicate that CDots-induced EMT could facilitate the formation of the epidermal barrier (Figure 8c1, red arrows in Figure 8c4, and blue arrows in Figure S11a,b, Supporting Information), thus blocking the secretion of excessive collagen and the occurrence of the hyalinization.

On day 21, it is found that the scar formation of the CDots group is significantly less than that of the control group (white arrows in Figure 8c3,c6),^[67] indicating the better healing quality in CDots group. Last, the images of H&E staining of important organs in the CDots group, including hearts, livers, spleens and kidneys, indicate that cell morphologies show no difference compared to the control group, suggesting that CDots are safe for in vivo applications (Figure S12, Supporting Information).

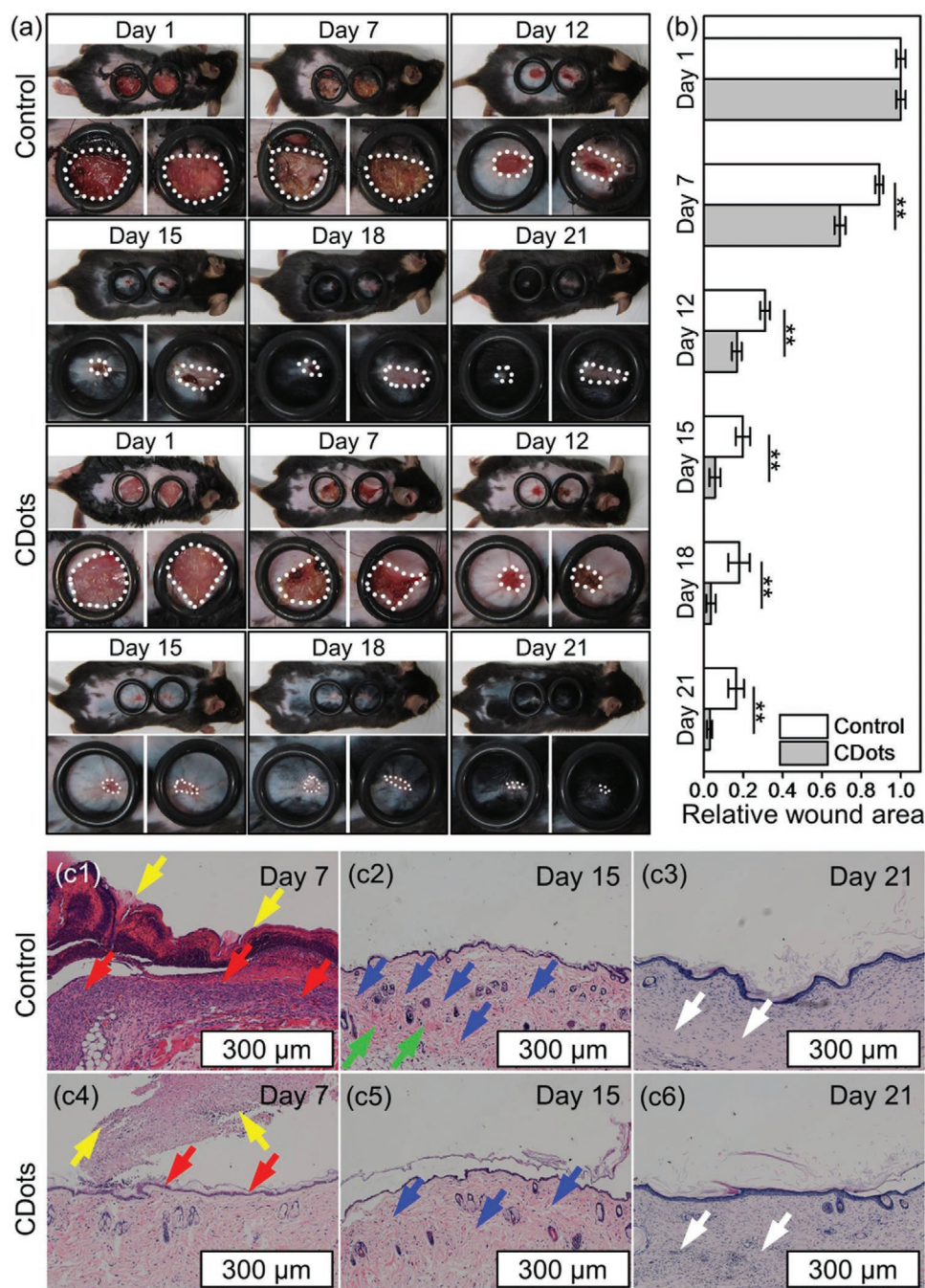


Figure 8. In vivo wound healing assay and histological evaluation. a) Photographs of full-thickness cutaneous wounds on day 1, 7, 12, 15, 18, and 21. b) Corresponding quantitative data of the relative wound area on these time points was analyzed using ImageJ software. The relative wound area was defined as the ratio of the wound area of different time points to the initial wound area. c) Histological evaluation on day 7, 15, and 21. Yellow arrows: scabs; red arrows: inflammation and epithelium; blue arrows: collagen fibers; green arrows: hyalinization; white arrows: scars. Data are presented as mean \pm SD from three experiments. * indicates $P < 0.05$; ** indicates $P < 0.01$.

Furthermore, the comparison of CDots with the commercial wound healing medicine is carried out (Figure S13, Supporting Information). In the pharmaceutical market, the major commercial wound healing medicines are mostly based on the growth factors, such as epidermal growth factor (EGF) and fibroblast growth factor (FGF), whereas TGF- β is not the major commercial wound healing molecule because of its high

cost. Therefore, the commercial EGF and FGF, which hold most wound healing market share, are selected to evaluate the capacity of promoting wound healing comparing with CDots in vivo. The English names of these two commercial wound healing substances are “Recombinant human epidermal growth factor derivative for external use, liquid (I)” and “Recombinant bovine basic fibroblast growth factor for external use, liquid,”

respectively, where their active ingredients (i.e., EGF and FGF) are adopted to stand for these two commercial pharmaceuticals in following discussions. In the animal experiment, the male C57BL/6 mice (four to six-week-old) possessing full-thickness cutaneous wounds are randomly divided into four groups, namely control, EGF, FGF and CDots groups. The method of the animal experiment is identical with the section of the animal experiment in this manuscript, and their dosages are determined based on the package insert. The commercial EGF and FGF are recommended for being sprayed on the wound surface according to the package insert, but the application of the medicine will be blocked by the scabs formed in the follow-up treatment, leading to the reduction of the efficacy of EGF and FGF. Thus, the intradermal injection is used to avoid the effect of the scabs.

As shown in Figure S13a (Supporting Information), the representative digital photographs of the wounds in the four groups are taken on day 1, 7, 12, 15, 18, and 21, respectively. The images indicate no significant difference among these four groups on day 1. On day 7, there are no significant differences in the wound area among the CDots, EGF and FGF groups, however, these three groups achieve a significantly larger reduction compared with the control group in wound area. Figure S13b (Supporting Information) shows the quantification of the corresponding wound area upon different treatments. Similar to the situation of day 7, the CDots, EGF and FGF groups show no significant differences in the wound area on day 12, but compared to the initial wound area, they decreased to 19% while the control group remains 36%. These results illustrate the wound healing rates are significantly promoted by these three substances. On day 15, the wounds in the CDots, EGF and FGF groups have almost healed up and there are few scars formed. However, the wound area of the control group still keeps large (33%). Finally, the wound healing in the control group is completed with massive scar formation on day 21. These results demonstrate that CDots, EGF and FGF can significantly accelerate the wound healing process compared to control group and the efficacy of CDots is comparable to those of the commercial EGF and FGF in promoting wound healing in vivo.

To get more insight into wound healing in the CDots, EGF and FGF groups, H&E staining of the wound site tissue is also carried out. The H&E staining image shows no re-epithelialization formed in the control group, but there are still considerable inflammatory cells and excessive granulation tissue and plenty of scabs connected to the granulation tissue in wound on day 7 (Figure S14a1, Supporting Information). In comparison, in the CDots, EGF and FGF groups, a balanced amount of granulation tissue and an obvious re-epithelialization can be seen, the inflammatory cell infiltration under the epidermis is much less, and the scabs have fallen off (Figure S14a2–a4, Supporting Information). On day 15, excessive collagen secreted by excessive granulation tissues under the external stimuli and the occurrence of hyalinization could be observed in the control group (Figure S14b1, Supporting Information). In contrast, the CDots, EGF and FGF groups show a reasonable amount of collagen secreted, which is meaningful for wound healing (Figure S14b2–b4, Supporting Information). On day 21, it is found that the scar formation in

the CDots, EGF and FGF groups is significantly less than that in the control group, demonstrating the better healing quality in the CDots, EGF and FGF groups (Figure S14c1–c4, Supporting Information). These results further prove that CDots can efficiently promote wound healing with a good healing quality, which is comparable to those of the commercial EGF and FGF.

Besides the efficacy, the cost of the medicine is another important concern in research and practical applications. According to the calculation (Table S1, Supporting Information), the cost per wound of using CDots is much lower than those of the commercial wound healing medicines, indicate that our synthesized CDots hold great potential as a novel nanoparticle-based medicine for promoting wound healing.

3. Conclusion

In summary, we synthesized CDots via microwave-assisted heating ascorbic acid and PEI. The resulting CDots with abundant carboxyl and amine groups exhibited excellent biocompatibility, and can induce the EMT process by activating TGF- β /p38/Snail signaling pathway, leading to the increase of cell motility. In vivo studies revealed that CDots could accelerate the migration of epithelial cells in the full-thickness cutaneous wounds through triggering EMT, leading to a rapid re-epithelialization covering the granulation tissue and the formation of epidermal barrier thereof, which can block the external stimuli, reduce the inflammatory reaction and the granulation tissue, and finally promote the wound healing as well as few scar formation. We believe that the CDots demonstrated here may be widely used in developing novel nanoparticles-based medicine, and further open up new avenues of discovery in pharmaceutical research.

4. Experimental Section

Materials: Ascorbic acid (99.99%), polyethyleneimine (PEI, MWCO = 1800 D, 99%), fetal bovine serum (FBS), and human immortalized keratinocytes (HaCaT) were purchased from Macklin (Shanghai, China), Aladdin Ltd. (Shanghai, China), Biological Industries (Cromwell, CT, USA), and KeyGEN BioTECH (Nanjing, China), respectively. Dulbecco's modified Eagle medium (DMEM) with high glucose and penicillin-streptomycin were obtained from Hyclone (Logan, UT, USA). Two kinds of traditional wound healing medicines were commercially available products and used as received, where their English names are "Recombinant human epidermal growth factor derivative for external use, liquid (I)" and "Recombinant bovine basic fibroblast growth factor for external use, liquid," respectively. SB-431542 and 1-5-*tert*-butyl-2-p-tolyl-2H-pyrazol-3-yl)-3-[4-(2-morpholin-4-yl-ethoxy)naphthalen-1-yl] urea (BIRB 796) were obtained from Selleck Chemicals LLC (Houston, TX, USA). Apoptosis analysis kit and 3-(4,5-dimethyl-2-thiazolyl)-2,5-diphenyl-2-*H*-tetrazolium bromide (MTT) were obtained from Sungene Biotech (Tianjin, China) and Amresco (Solon, OH, USA), respectively. Sodium dodecyl sulfate polyacrylamide gel electrophoresis (SDS-PAGE), radioimmunoprecipitation assay (RIPA) buffer, 4,6-diamidino-2-phenylindole (DAPI) and bovine serum albumin (BSA) were from Beyotime (Shanghai, China). Protease and phosphatase inhibitor cocktail were from MedChemExpress LLC (Monmouth Junction, NJ, USA). Primary antibodies were from Santa Cruz Biotechnology (Dallas, TX, USA), Proteintech (Rosemont, IL, USA) and Cell Signaling Technology

(CST, Danvers, MA, USA). Secondary antibodies and Cy3-labeled IgG antibody were obtained from Proteintech (Rosemont, IL, USA). Western blot stripping buffer was from Thermo Fisher Scientific (Waltham, MA, USA). C57BL/6 mice were obtained from Liaoning Changsheng biotechnology Co. (Benxi, China). Dialysis bag (MWCO = 3500 D) was obtained from Spectrum Laboratories (Rancho Dominguez, CA, USA). Transwell chambers were obtained from Corning Costar (New York USA).

Synthesis and Purification of Carbon Dots (CDots): Briefly, 1 g of ascorbic acid and 0.5 g of PEI were dissolved in 20 mL of deionized water and then microwaved for 4 min in a domestic 500 W microwave oven. During this process, the color of the solution changed from a colorless liquid to a light yellow color, and finally to a dark brown solid (i.e., CDots). After being cooled in the air, the as-prepared CDots were dissolved in 30 mL of deionized water and then centrifuged at 8000 rpm for 5 min to remove agglomerated particles. To further purify the CDots, the CDots aqueous solution was dialyzed in deionized water for 24 h using a dialysis bag to get rid of unreacted reagents and other small by-product. Finally, the purified CDots aqueous solution was condensed in a vacuum rotary evaporator, and CDots were re-dissolved in deionized water for further use.

Characterization of CDots: Ultraviolet–visible (UV–vis) absorption spectra were acquired using a Lambda 800 UV–vis spectrophotometer. A Shimadzu RF-5301 PC spectrophotometer was used to obtain the photoluminescence spectroscopy (PL) spectroscopy. Images of high-resolution transmission electron microscopy were taken using a Hitachi H-800 electron microscope at an acceleration voltage of 200 kV with a CCD camera. An Inca X-Max instrument (Oxford Instruments) was applied to measure energy dispersive spectra. A Nicolet AVATAR 360 Fourier transform infrared (FTIR) instrument was used to acquire the FTIR spectra. X-ray photoelectron spectroscopy was obtained using a VG ESCALAB MKII spectrometer with a Mg KR excitation (1253.6 eV). Binding energy calibration was based on C 1s at 284.6 eV. Confocal laser scanning microscopy (CLSM) images were taken using an Olympus Fluoview FV1000. MTT measurements were carried out using a micro-plate reader RT-6000 from Rayto Life and Analytical Sciences Co. (Shenzhen, China). Optical images of cultured cells were taken using an Olympus BX-51 inverted fluorescence microscope (Tokyo, Japan) with a CCD camera.

Ninhydrin Reaction: 0.2 g of ninhydrin (Aladdin) was dissolved in 10 mL of CDots solution and mixed. After that, the mixed solution was heated at 60 °C for 10 min. The UV–vis absorption spectra were acquired and the photographs were taken before and after treating the CDots solution.

Cell Culture: HaCaT cells were cultured in DMEM containing 10% FBS, 100 U mL⁻¹ penicillin and 100 µg mL⁻¹ streptomycin in a 5% CO₂ humidified incubator at 37 °C. The medium was changed every 2–3 days.

Cytotoxicity Assays: HaCaT cells were seeded at 1 × 10⁴ cells per well in a 96-well plate and cultured overnight. Then the medium was removed, and 200 µL of medium containing different concentrations of CDots (200, 400, and 600 µg mL⁻¹) was added to each well. After 24 h, 20 µL of MTT (5 µg mL⁻¹) was added to each well and incubated for another 4 h. Finally, the medium was replaced with 150 µL dimethyl sulfoxide, and a microplate reader was used to measure the absorbance at a wavelength of 490 nm. The cell viability was presented as a percentage of the control group. HaCaT cells were seeded at 2 × 10⁵ cells per well in a 6-well plate and cultured overnight. Then the medium was replaced with 2 mL medium contained different concentrations of CDots (200, 400, and 600 µg mL⁻¹). After 24 h, cells were collected and washed twice with chilled PBS and resuspended in 100 µL of binding buffer. Finally, the cells were stained by annexin V-FITC/7AAD apoptosis assay kit (Tianjin Sungene Biotech Co., Tianjin, China) according to the manufacturer's instructions and analyzed by fluorescence-activated cell sorting (FACS, BD Biosciences, San Jose, CA, USA).

Western Blot: HaCaT cells were seeded in a 6-well plate and cultured overnight. Then the medium was replaced with 2 mL medium containing different concentrations of CDots (200, 400, and 600 µg mL⁻¹). After 24 h, cells were lysed in RIPA buffer to obtain cellular protein. The protein extracts were run on SDS-PAGE and then transferred on polyvinylidene fluoride membrane. The blot was blocked with 5% BSA for 1 h at room

temperature, and incubated with primary antibodies overnight at 4 °C. The following primary antibodies were used: anti-GAPDH (10494-1-AP, 1:2000 (Proteintech)), anti-E-cadherin (20874-1-AP, 1:5000 (Proteintech)), anti-vimentin (10366-1-AP, 1:1000 (Proteintech)), anti-fibronectin (15613-1-AP, 1:1000 (Proteintech)), anti-Snail (13099-1-AP, 1:1000 (Proteintech)), anti-p-Smad2 (3104, 1:1000 (CST)), anti-p-Smad3 (9520, 1:1000 (CST)), anti-Smad2/3 (3102, 1:1000 (CST)), anti-p-Erk (9101, 1:1000 (CST)), anti-Erk (4695, 1:1000 (CST)), anti-p-JNK (9251, 1:1000 (CST)), anti-JNK (9252, 1:1000 (CST)), anti-p-p38 (9211, 1:1000 (CST)), anti-p38 (9212, 1:1000 (CST)), anti-p-Tyr (PY99) (sc-7020, 1:1000 (Santa Cruz)), and anti-TGF-β RII (sc-17791, 1:500 (Santa Cruz)). Afterward, secondary antibodies were added and incubated for 1 h at room temperature. The blot was stripped by stripping buffer according to the user guide. The signal was detected using enhanced chemiluminescence reagent, and band density was analyzed by ImageJ software. To further evaluate the roles of transforming growth factor-β (TGF-β) and p-38 mitogen-activated kinase (p38) in CDots-induced EMT, SB-431542 and BIRB 796 were added and the same procedure was used.

Immunofluorescence Staining and Fluorescence Colocalization: HaCaT cells were seeded on coverslips at 1 × 10⁵ cells per well in a 6-well plate or confocal dishes and cultured overnight. Then the medium was replaced with 2 mL medium containing different concentrations of CDots (200, 400, and 600 µg mL⁻¹). After 24 h, the cells were fixed with methanol for 20 min at room temperature. Nonspecific binding sites were blocked with 5% BSA for 1 h. Afterward, the cells were incubated with E-cadherin antibody (20874-1-AP, 1:500 (Proteintech)) and vimentin antibody (10366-1-AP, 1:500 (Proteintech)) for immunofluorescence staining and anti-TGF-β RII (sc-17791, 1:200 (Santa Cruz)) for fluorescence co-localization at 4 °C overnight, respectively. Cy3-labeled secondary antibody was added and incubated for 1 h at room temperature in the dark. Then, the cells were stained with 4,6-diamidino-2-phenylindole (DAPI) for 5 min, and observed by an inverted fluorescence microscope and CLSM.

siRNA Transfection and Reverse Transcriptase Quantitative Polymerase Chain Reaction (RT-qPCR) Assay: The HaCaT cells were cultured in 6-well plates with 2 mL of medium. The siRNA of TGF-β (Sangon Biotech) and transfection reagent (Lipofectamine 2000, Thermo Fisher Scientific) were mixed in serum free medium for 5 min at room temperature. After that, the medium of the HaCaT cells was replaced by the mixed medium and cultured for 24 h. RNeasy mini purification kit and iScript cDNA synthesis kit were used to extract total RNA and synthesize cDNAs, respectively. SYBR Premix Ex Taq and MxPro Mx3005P real-time PCR detection system (Agilent Technologies, Santa Clara, CA) were used to conduct qPCR assays and ACTB was used as an internal control.

Cell Migration Assay: The 24-well transwell chambers equipped with polycarbonate membranes (pore size = 8 µm in diameter) were used to evaluate the migration ability. HaCaT cells were incubated with different concentrations of CDots (200, 400, and 600 µg mL⁻¹) for 24 h. Then the cells were collected and seeded at 5 × 10⁴ cells per well in the upper chambers and cultured with DMEM. DMEM containing 10% FBS was added to the lower chambers. After 24 h, the cells on inferior membrane were fixed with methanol and stained with crystal violet. The images of cells were taken by a microscope. To further evaluate the roles of TGF-β and p38 in CDots-induced EMT, siRNA, another two kinds of CDots, SB-431542 and BIRB 796 were added and the same procedure was used.

Scratch Assay: HaCaT cells were seeded at 2 × 10⁵ cells per well in 6-well plate and cultured until complete confluence. Three parallel scratches were made with a pipette tip in each well, and the area of the scratch was measured. Then the medium was removed, and 2 mL of FBS-free medium containing different concentrations of CDots (200, 400, and 600 µg mL⁻¹) was added to each well. After 24 h, the cells were fixed with methanol and stained with crystal violet. Images of scratched area were taken. The scratched area was observed by a microscope and analyzed using ImageJ software.

Animal Experiments: All animal experiments were performed in accordance with the Guidelines for the Care and Use of Laboratory Animals of Jilin University and approved by the Animal Ethics Committee of Jilin University. 8 male C57BL/6 mice (four to six-week-old) were randomly divided into two groups, including control

and CDots ($n = 4$). The hair in the dorsal area of mice was shaved and sterilized, and then two round (10 mm diameter) full-thickness cutaneous wounds were created. A silicone ring was fixed around the wound to prevent contraction. Then the wounds were treated with 50 μL of DMEM or CDots (600 $\mu\text{g mL}^{-1}$) every three days until closure, respectively. Digital photographs of the wounds were taken on day 1, 7, 12, 15, 18, and 21. Skin and the subcutaneous tissues around the wound areas were excised on day 7, 15, and 21. Following a similar procedure, except using commercial wound healing medicines, the in vivo wound healing experiments were carried out for comparing the efficacy of CDots. Important organs of the control and CDots groups, including hearts, livers, spleens, and kidneys were collected on day 21. All the samples were stained with hematoxylin and eosin (H&E) staining as reported in a previous published paper. Skin and the subcutaneous tissues around the wound areas of the control and CDots groups on day 15 were excised and then stained with Masson's trichrome staining.

Statistical Analysis: All experiments were repeated at least 3 times. All the data were presented as mean \pm standard deviations (SD). First, the Levene's tests were performed for homogeneity of variance, which is a standard assumption of analysis of variance (ANOVA). The results of the tests indicated the P values are greater than 0.05, demonstrating the homogeneity of variance within each of the populations is equal (i.e., the homogeneity of variance is violated). One-way ANOVA followed by Bonferroni post hoc analysis was performed for the evaluation of statistical significances among the groups. $P < 0.05$ was regarded as statistical significance.

Supporting Information

Supporting Information is available from the Wiley Online Library or from the author.

Acknowledgements

Z.W. and L.L. contributed equally to this work. This work was supported by grants from the National Key Research and Development Program of China 2016YFC1102800, the Natural Science Foundation of China (81920108012, 81870741 and 81970946), Young Elite Scientist Sponsorship Program by CAST (2018QNRC001), China Postdoctoral Science Foundation (2018T110259 and 2016M601386), Jilin Province Education Department Science and Technology Research (JJKH20190106KJ), Jilin Province Science and Technology Research (20190103088JH, 20200201611JC), Jilin Province Finance Department Science and Technology Research (JCSZ2019378-30), Jilin Province Health Department Youth Science and Technology Research (2019Q014), Open Project of State Key Laboratory of Supramolecular Structure and Materials (sklssm202038), State Key Laboratory of Luminescence and Applications (SKLA-2020-07), and JLU Science and Technology Innovative Research Team (2017TD-11).

Conflict of Interest

The authors declare no conflict of interest.

Keywords

carbon dots, epithelial-mesenchymal transition, nanomaterials, wound healing

Received: June 9, 2020
Published online: September 4, 2020

- [1] Y. Belkaid, J. A. Segre, *Science* **2014**, *346*, 954.
- [2] C. C. Finnerty, M. G. Jeschke, L. K. Branski, J. P. Barret, P. Dziewulski, D. N. Herndon, *Lancet* **2016**, *388*, 1427.
- [3] M. Wang, C. G. Wang, M. Chen, Y. W. Xi, W. Cheng, C. Mao, T. Z. Xu, X. X. Zhang, C. Lin, W. Y. Gao, Y. Guo, B. Lei, *ACS Nano* **2019**, *13*, 10279.
- [4] P. Rousselle, F. Braye, G. Dayan, *Adv. Drug Delivery Rev.* **2019**, *146*, 344.
- [5] H. S. Kim, X. Y. Sun, J. H. Lee, H. W. Kim, X. B. Fu, K. W. Leong, *Adv. Drug Delivery Rev.* **2019**, *146*, 209.
- [6] J. Coyne, N. Zhao, A. Olubode, M. Menon, Y. Wang, *J. Controlled Release* **2020**, *318*, 185.
- [7] N. Li, L. Q. Yang, C. L. Pan, P. E. Saw, M. Ren, B. Y. Lan, J. F. Wu, X. Y. Wang, T. T. Zeng, L. Y. Zhou, L. M. Zhang, C. Yang, L. Yan, *Acta Biomater.* **2020**, *102*, 298.
- [8] N. A. Agabalyan, H. D. Sparks, S. Tarraf, N. L. Rosin, K. Anker, G. Yoon, L. N. Burnett, D. Nickerson, E. S. Di Martino, V. A. Gabriel, J. Biernaskie, *Stem Cell Rep.* **2019**, *13*, 1068.
- [9] B. R. Griffin, C. C. Frear, F. Babl, E. Oakley, R. M. Kimble, *Ann. Emerg. Med.* **2020**, *75*, 75.
- [10] M. Ashtikar, M. G. Wacker, *Adv. Drug Delivery Rev.* **2018**, *129*, 194.
- [11] D. Haensel, X. Dai, *Dev. Dyn.* **2018**, *247*, 473.
- [12] H. Pratsinis, E. Mavroganatos, D. Kletsas, *Adv. Drug Delivery Rev.* **2019**, *146*, 325.
- [13] A. Ravikrishnan, T. Ozdemir, M. Bah, K. A. Baskerville, S. I. Shah, A. K. Rajasekaran, X. Jia, *ACS Appl. Mater. Interfaces* **2016**, *8*, 17915.
- [14] F. Lv, J. Wang, P. Xu, Y. M. Han, H. S. Ma, H. Xu, S. J. Chen, J. Chang, Q. F. Ke, M. Y. Liu, Z. F. Yi, C. T. Wu, *Acta Biomater.* **2017**, *60*, 128.
- [15] K. Singh, M. Sinha, D. Pal, S. Tabasum, S. C. Gnyawali, D. Khona, S. Sarkar, S. K. Mohanty, F. Soto-Gonzalez, S. Khanna, S. Roy, C. K. Sen, *Diabetes* **2019**, *68*, 2175.
- [16] D. Q. Pei, X. D. Shu, A. Gassama-Diagne, J. P. Thiery, *Nat. Cell Biol.* **2019**, *21*, 44.
- [17] M. A. Nieto, R. Y. J. Huang, R. A. Jackson, J. P. Thiery, *Cell* **2016**, *166*, 21.
- [18] S. W. Stoll, L. Rittié, J. L. Johnson, J. T. Elder, *J. Invest. Dermatol.* **2012**, *132*, 2148.
- [19] L. Yu, M. C. Hébert, Y. E. Zhang, *EMBO J.* **2002**, *21*, 3749.
- [20] B. Ozdamar, R. Bose, M. Barrios-Rodiles, H. R. Wang, Y. Zhang, J. L. Wrana, *Science* **2005**, *307*, 1603.
- [21] N. Q. Gong, X. W. Ma, X. X. Ye, Q. F. Zhou, X. A. Chen, X. L. Tan, S. K. Yao, S. D. Huo, T. B. Zhang, S. Z. Chen, X. C. Teng, X. X. Hu, J. Yu, Y. L. Gan, H. D. Jiang, J. H. Li, X. J. Liang, *Nat. Nanotechnol.* **2019**, *14*, 379.
- [22] M. I. Setyawati, C. Sevensan, B. H. Bay, J. P. Xie, Y. B. Zhang, P. Demokritou, D. T. Leong, *Small* **2018**, *14*, 1800922.
- [23] P. Wang, Y. Wang, X. Nie, C. Braïni, R. Bai, C. Y. Chen, *Small* **2015**, *11*, 446.
- [24] R. B. Li, X. Wang, Z. X. Ji, B. B. Sun, H. Y. Zhang, C. H. Chang, S. J. Lin, H. Meng, Y. P. Liao, M. Y. Wang, Z. X. Li, A. Hwang, T. B. Song, R. Xu, Y. Yang, J. I. Zink, A. E. Nel, T. Xia, *ACS Nano* **2013**, *7*, 2352.
- [25] T. Chen, H. Y. Nie, X. Gao, J. L. Yang, J. Pu, Z. J. Chen, X. X. Cui, Y. Wang, H. F. Wang, G. Jia, *Toxicol. Lett.* **2014**, *226*, 150.
- [26] M. Polimeni, G. R. Gulino, E. Gazzano, J. Kopecka, A. Marucco, I. Fenoglio, F. Cesano, L. Campagnolo, A. Magrini, A. Pietroiusti, D. Ghigo, E. Aldieri, *Part. Fibre Toxicol.* **2015**, *13*, 27.
- [27] P. Wang, M. Voronkova, S. Luanpitpong, X. Q. He, H. Riedel, C. Z. Dinu, L. Y. Wang, Y. Rojanasakul, *Chem. Res. Toxicol.* **2017**, *30*, 1396.
- [28] J. Ma, B. Bishoff, R. R. Mercer, M. Barger, D. Schwegler-Berry, V. Castranova, *Toxicol. Appl. Pharmacol.* **2017**, *323*, 16.
- [29] X. W. Xu, K. Zhang, L. Zhao, C. Li, W. H. Bu, Y. Q. Shen, Z. Y. Gu, B. Chang, C. Y. Zheng, C. T. Lin, H. C. Sun, B. Yang, *ACS Appl. Mater. Interfaces* **2016**, *8*, 32706.
- [30] J. J. Liu, S. Y. Lu, Q. L. Tang, K. Zhang, W. X. Yu, H. C. Sun, B. Yang, *Nanoscale* **2017**, *9*, 7135.

- [31] H. Ding, J. S. Wei, P. Zhang, Z. Y. Zhou, Q. Y. Gao, H. M. Xiong, *Small* **2018**, *14*, 1800612.
- [32] L. Xiao, H. D. Sun, *Nanoscale Horiz.* **2018**, *3*, 565.
- [33] D. Y. Shan, J. T. Hsieh, X. C. Bai, J. Yang, *Adv. Healthcare Mater.* **2018**, *7*, 1800532.
- [34] F. Ostadhosseini, L. Benig, I. Tripathi, S. K. Misra, D. Pan, *ACS Appl. Mater. Interfaces* **2018**, *10*, 19408.
- [35] J. P. Li, S. W. Yang, Y. Deng, P. W. Chai, Y. C. Yang, X. Y. He, X. M. Xie, Z. H. Kang, G. Q. Ding, H. F. Zhou, X. Q. Fan, *Adv. Funct. Mater.* **2018**, *28*, 1800881.
- [36] D. K. Khajuria, V. B. Kumar, D. Gigi, A. Gedanken, D. Karasik, *ACS Appl. Mater. Interfaces* **2018**, *10*, 19373.
- [37] Q. Y. Jia, J. C. Ge, W. M. Liu, X. L. Zheng, S. Q. Chen, Y. M. Wen, H. Y. Zhang, P. F. Wang, *Adv. Mater.* **2018**, *30*, 1706090.
- [38] Z. F. Wang, F. L. Yuan, X. H. Li, Y. H. Li, H. Z. Zhong, L. Z. Fan, S. H. Yang, *Adv. Mater.* **2017**, *29*, 1702910.
- [39] J. C. Liu, N. Wang, Y. Yu, Y. Yan, H. Y. Zhang, J. Y. Li, J. H. Yu, *Sci. Adv.* **2017**, *3*, 1603171.
- [40] S. Kalytchuk, K. Polakova, Y. Wang, J. P. Froning, K. Cepe, A. L. Rogach, R. Zboril, *ACS Nano* **2017**, *11*, 1432.
- [41] Y. H. Chen, M. T. Zheng, Y. Xiao, H. W. Dong, H. R. Zhang, J. L. Zhuang, H. Hu, B. F. Lei, Y. L. Liu, *Adv. Mater.* **2016**, *28*, 312.
- [42] K. Jiang, S. Sun, L. Zhang, Y. Lu, A. G. Wu, C. Z. Cai, H. W. Lin, *Angew. Chem., Int. Ed.* **2015**, *54*, 5360.
- [43] M. L. Liu, B. B. Chen, C. M. Li, C. Z. Huang, *Green Chem.* **2019**, *21*, 449.
- [44] C. Zhu, Y. J. Fu, C. G. Liu, Y. Liu, L. L. Hu, J. Liu, I. Bello, H. Li, N. Y. Liu, S. J. Guo, H. Huang, Y. Lifshitz, S. T. Lee, Z. H. Kang, *Adv. Mater.* **2017**, *29*, 1701399.
- [45] S. Chaudhary, A. Umar, K. K. Bhasin, S. Singh, *J. Biomed. Nanotechnol.* **2017**, *13*, 591.
- [46] S. N. Qu, X. Y. Liu, X. Y. Guo, M. H. Chu, L. G. Zhang, D. Z. Shen, *Adv. Funct. Mater.* **2014**, *24*, 2689.
- [47] X. T. Tian, X. B. Yin, *Small* **2019**, *15*, 1901803.
- [48] K. Bankoti, A. P. Rameshbabu, S. Datta, B. Das, A. Mitra, S. Dhara, *J. Mater. Chem. B* **2017**, *5*, 6579.
- [49] M. Omid, A. Yadegari, L. Tayebi, *RSC Adv.* **2017**, *7*, 10638.
- [50] I. Onyekwelu, R. Yakkanti, L. Protzer, C. M. Pinkston, C. Tucker, D. Seligson, *JAAOS: Global Res. Rev.* **2017**, *1*, 022.
- [51] D. Zhou, P. T. Jing, Y. Wang, Y. C. Zhai, D. Li, Y. Xiong, A. V. Baranov, S. N. Qu, A. L. Rogach, *Nanoscale Horiz.* **2019**, *4*, 388.
- [52] P. A. Kendall, *Nature* **1963**, *197*, 1305.
- [53] S. Liarte, Á. Bernabé-García, F. J. Nicolás, *Cells* **2020**, *9*, 255.
- [54] J. Yue, K. M. Mulder, *Pharmacol. Ther.* **2001**, *91*, 1.
- [55] B. M. Chacko, B. Y. Qin, A. Tiwari, G. Shi, S. Lam, L. J. Hayward, M. De Caestecker, K. Lin, *Mol. Cell* **2004**, *15*, 813.
- [56] Y. E. Zhang, *Cell Res.* **2009**, *19*, 128.
- [57] Y. Kuma, G. Sabio, J. Bain, N. Shpiro, R. Márquez, A. Cuenda, *J. Biol. Chem.* **2005**, *280*, 19472.
- [58] R. Derynck, X. H. Feng, *Biochim. Biophys. Acta* **1997**, *1333*, F105.
- [59] A. P. Hinck, *FEBS Lett.* **2012**, *586*, 1860.
- [60] A. P. Hinck, T. D. Mueller, T. A. Springer, *Cold Spring Harbor Perspect. Biol.* **2016**, *8*, a022103.
- [61] S. J. Lin, T. F. Lerch, R. W. Cook, T. S. Jardetzky, T. K. Woodruff, *Reproduction* **2006**, *132*, 179.
- [62] J. L. Wrana, L. Attisano, R. Wieser, F. Ventura, J. Massagué, *Nature* **1994**, *370*, 341.
- [63] N. Q. McDonald, R. Lapatto, J. Murray-Rust, J. Gunning, A. Wlodawer, T. L. Blundell, *Nature* **1991**, *354*, 411.
- [64] D. Zhou, Y. C. Zhai, S. N. Qu, D. Li, P. T. Jing, W. Y. Ji, D. Z. Shen, A. L. Rogach, *Small* **2017**, *13*, 1602055.
- [65] I. Pastar, O. Stojadinovic, N. C. Yin, H. Ramirez, A. G. Nusbaum, A. Sawaya, S. B. Patel, L. Khalid, R. R. Isseroff, M. Tomic-Canic, *Adv. Wound Care* **2014**, *3*, 445.
- [66] J. J. Gan, C. Y. Liu, H. L. Li, S. C. Wang, Z. Z. Wang, Z. Q. Kang, Z. Huang, J. F. Zhang, C. M. Wang, D. L. Lv, L. Dong, *Biomaterials* **2019**, *219*, 119340.
- [67] M. L. Xue, C. J. Jackson, *Adv. Wound Care* **2015**, *4*, 119.
- [68] S. Ahn, H. A. M. Ardoña, P. H. Campbell, G. M. Gonzalez, K. K. Parker, *ACS Appl. Mater. Interfaces* **2019**, *11*, 33535.
- [69] G. Z. Lu, Z. Z. Ding, Y. Y. Wei, X. H. Lu, Q. Lu, D. L. Kaplan, *ACS Appl. Mater. Interfaces* **2018**, *10*, 44314.